Physical electronics

Original article
UDC 621.385.6
DOI: https://doi.org/10.18721/JPM.16410

ENHANCEMENT OF THE 4-mm WAVELENGTH GYROTRON EFFICIENCY BY MULTISTAGE ENERGY RECOVERY

O. I. Louksha ✉, P. A. Trofimov, A. G. Malkin

Peter the Great St. Petersburg Polytechnic University, St. Petersburg, Russia

✉ louksha@rphf.spbstu.ru

Abstract. This study presents the results of a complex physical modeling of a moderate power gyrotron operating at the 4-mm wavelength range. The characteristics of electrodes and magnetic coils in a four-stage recovery collector were optimized taking into account the coordinate and velocity distributions of electrons. These distributions were obtained through a trajectory analysis in the electron optical system and calculation of electron-wave interaction in the gyrotron cavity. To reduce parasitic effects of the bundles of a toroidal solenoid used to create an azimuthal magnetic field in the collector region, a sectioned electron beam was employed. The study demonstrated that the gyrotron's total efficiency of approximately 79 % could be achieved, being close to the maximum efficiency value achievable with separation of electron fractions with different energies, provided that the current of electrons reflected from a collector should not exceed 1% of the total current of an electron beam.

Keywords: microwave electronics, gyrotron, helical electron beam, recuperation, residual electron energy recovery

Funding: The reported study was funded by Russian Science Foundation (Grant No. 22-29-00136).

For citation: Louksha O. I., Trofimov P. A., Malkin A. G., Enhancement of the 4-mm wavelength gyrotron efficiency by multistage energy recovery, St. Petersburg State Polytechnical University Journal. Physics and Mathematics. 16 (4) (2023) 118–133. DOI: https://doi.org/10.18721/JPM.16410

Научная статья
УДК 621.385.6
DOI: https://doi.org/10.18721/JPM.16410

ПОВЫШЕНИЕ ЭФФЕКТИВНОСТИ ГИРОТРОНА С ДЛИНОЙ ВОЛНЫ 4 мм ЗА СЧЕТ МНОГОСТУПЕНЧАТОЙ РЕКУПЕРАЦИИ

О. И. Лукша ✉, П. А. Трофимов, А. Г. Малкин

Санкт-Петербургский политехнический университет Петра Великого,

Санкт-Петербург, Россия

✉ louksha@rphf.spbstu.ru

Аннотация. В работе представлены результаты комплексного физического моделирования гиротрона средней мощности, работающего на длине волны 4 мм. Проведена оптимизация характеристик электродов и магнитных катушек в коллекторе с четырехступенчатой рекуперацией с учетом распределения электронов по координатам и скоростям. Эти распределения были получены путем траекторного анализа в электронно-оптической системе и расчета электронно-волнового взаимодействия в резонаторе

гиротрона. Для снижения паразитного воздействия связок тороидального соленоида, используемого для создания азимутального магнитного поля в области коллектора, использован секционированный электронный пучок. Исследование показало, что можно получить общий КПД гиротрона около 79 %, что близко к максимальному значению, достижимому при идеальном разделении электронных фракций с разными энергиями, при условии, что ток отраженных от коллектора электронов не должен превышать 1 % от общего тока электронного пучка.

Ключевые слова: СВЧ-электроника, гиротрон, винтовой электронный поток, рекуперация, возвращение остаточной энергии электронов

Финансирование: Исследование выполнено при финансовой поддержке Российского научного фонда (грант № 22-29-00136).

Для цитирования: Лукша О. И., Трофимов П. А., Малкин А. Г. Повышение эффективности гиротрона с длиной волны 4 мм за счет многоступенчатой рекуперации // Научно-технические ведомости СПбГПУ. Физико-математические науки. 2023. Т. 16. № 4. С. 118–133. DOI: https://doi.org/10.18721/ JPM.16410

Introduction

In recent years, there has been an intensive search for new ways to improve powerful gyrotron-type devices due to the wide possibilities of their practical use. Gyrotrons occupy a leading position among effective sources of powerful microwave radiation in the millimeter and submillimeter wavelength ranges. They are irreplaceable in such an important application as electron-cyclotron plasma heating and current drive (ECH&CD) in magnetic confinement fusion systems designed to produce energy through controlled thermonuclear fusion (see, for example, Refs. [1 – 3]). The requirements to gyrotrons designed for thermonuclear fusion are exceptionally high. The ITER project requires gyrotrons operating at a frequency of 170 GHz, delivering an output power of approximately 1 MW and achieving a total efficiency exceeding 50 % [4]. The development of a new generation of nuclear fusion reactors will require resolving numerous physical and engineering tasks to improve gyrotrons performance. The DEMO project envisions usage of gyrotrons with a frequency exceeding 200 GHz and a total efficiency greater than 60 % at megawatt-level power [5]. Enhancement of device's energy efficiency simplifies dissipation of spent beam energy at collector, which is critical for reliable and long-time operation of high-power gyrotrons operating in the continuous wave (CW) regime. Achieving such high efficiencies is one of the primary objectives for developers of powerful gyrotrons today.

Increasing the gyrotrons' efficiency, as well as other vacuum sources of microwave radiation, can be achieved by recovering residual energy of spent electron beam in the collector. Almost all megawatt-level gyrotrons used in thermonuclear fusion systems are equipped by collectors with single-stage recovery which increase their total efficiency to 50 – 55% [6 – 8]. A further increase in efficiency is possible with multistage energy recovery systems. Such systems require spatial separation of electron beam fractions with different energies and deposition of these fractions on collector sections with different depressing potentials. However, to the best of our knowledge, no experiments have been conducted on gyrotrons with multistage recovery collector systems. The implementation of such systems has proven challenging due to specifics of velocity and coordinate distributions of electrons in helical electron beams (HEBs) of gyrotrons and due to the presence of residual magnetic field in collector region. A promising solution for spatial separation of electrons in gyrotron HEBs is the use of crossed electric and magnetic fields [9 – 11].

At Peter the Great St. Petersburg Polytechnic University (SPbPU), a possibility of electron separation in longitudinal electric and azimuthal magnetic fields has been proposed and investigated theoretically for development of gyrotrons with multistage recovery collectors [12].

The achievement of high gyrotrons' efficiency implies the high efficiency of transformation of electron energy to electromagnetic field energy in the cavity. The efficiency of this transformation is determined by quality of the HEB formed in the electron optical system. The research aimed

at improving the HEB quality was carried out at SPbPU using an experimental gyrotron with a frequency of 74.2 GHz and an output power of approximately 100 kW [13 – 15]. This gyrotron was equipped with unique diagnostic complex capable of measuring the HEB parameters and regulating distributions of electric and magnetic fields in electron optical system. The initial version of a four-stage recovery collector for this gyrotron was described in Ref. [16]. In this work, the collector system geometry was significantly modified and distributions of electric and magnetic fields were optimized, resulting in a noticeable enhancement of residual energy recovery efficiency. The multistage recovery system described in this paper has already been implemented in the SPbPU gyrotron.

This article is organized as follows.

Section I presents the results of trajectory analysis of the HEB in the electron optical system of the gyrotron. The approach that considers initial spread of electron velocities caused by roughness of cathode surface and by thermal velocity spread was implemented [17]. Regulation of electric field distribution in the cathode region allowed to increase the HEB's quality and maximum average pitch factor.

Section II describes the results of the Particle-in-Cell (PIC) simulation in the cavity region of the gyrotron using the input HEB parameters determined from the trajectory analysis in the electron optical system. The output radiation parameters at $TE_{12,3}$ operating mode and the characteristics of spent electron beam entering the collector region were obtained in this simulation.

Section III presents the results of trajectory analysis in the four-stage recovery collector, where parameters of electrodes and magnetic coils were optimized to achieve the maximum recovery efficiency and to minimize the current of electrons reflected from the collector. All calculations were performed using the CST Studio Suite software. Specifics of conducting calculations in CST Studio Suite, such as model construction, meshing, choice of computational parameters, etc., employed in this study, were similar to those described earlier in Refs. [16, 18].

I. Electron optical system

Table 1 shows the parameters of the SPbPU gyrotron operating regime. Fig. 1 shows a schematic drawing of the electron optical system elements in the r–z plane, including calculated electron trajectories. An electron beam in the gyrotron is formed using a three-electrode magnetron-injection gun (MIG). Thus, it is possible to modify parameters of the HEB by varying the voltage U_a between the anode and device's body. The accelerating voltage U_0 between the cathode and body which determines an average electron energy in the HEB remained constant at 30 kV during the calculations described below. The cathode assembly includes a control electrode positioned behind the cathode emissive strip, which can be used to optimize distribution of electric field in the cathode region and to minimize the velocity spread of electrons by adjusting the voltage at control electrode U_{cont} [19]. At the values of U_0, B_0, B_c and I_b indicated in Table 1 and in the case of $U_a = 0$ and $U_{cont} = 0$, the average pitch factor of electrons α was approximately 1.3. All HEB parameters mentioned in this section were determined in the central plane of the cavity $z = 260.5$ mm (see Fig. 1). The objective of trajectory analysis in the electron optical system was to achieve a high pitch factor ($\alpha > 1.5$) with a low velocity spread and minimal electron reflection from the magnetic mirror by regulating the voltages U_a and U_{cont}. Additionally, the magnetic compression coefficient B_0/B_c was varied by adjusting the magnetic field induction near cathode B_c to ensure optimal beam radius in the cavity (see Section II).

The present calculations differ from the previous ones described in Ref. [16] by taking into account initial electron velocity spread caused by roughness of cathode surface and thermal velocity spread. As shown in Ref. [17], the velocity characteristics of electrons in the beam can be made approximately coincided for two cathode models: (a) a rough cathode with inhomogeneities on its surface in the form of micron-sized hemispheres with radius r_0 and (b) a smooth cathode with Maxwell distribution of the initial velocities at an increased effective cathode temperature T^* and a spread of the angle φ between the direction of the initial velocity vector and direction of the normal. The angle φ is uniformly distributed in the range from $-\Delta\varphi$ to $+\Delta\varphi$. For instance, an initial transverse velocity spread is the same for the model (a) at $r_0 = 14$ μm and for the model (b) at $T^* = 67\,000$ K and $\Delta\varphi = \pm 90°$. Therefore, at the appropriate values of T^* and $\Delta\varphi$ the velocity spread factor associated with roughness of the cathode surface can be taken into account when performing a three-dimensional trajectory analysis in the electron optical gyrotron system

with a smooth cathode. It should be noted that at the T^* value being much higher than the actual cathode temperature T_c, the average electron energy in the HEB $\langle W \rangle$ and the energy spread δW additionally increase. An increase in the average energy can be compensated by changing of the accelerating voltage. The additional energy spread δW is much less than the energy spread caused by the beam potential depression [16]. Since $T^* >> T_c$, an initial velocity spread set within the framework of this model can be considered as being caused by the combined effect of roughness of cathode surface and the thermal velocity spread. Further simulations were carried out at $T^* = 67\ 000$ K and $\Delta\varphi = \pm 90°$. At such T^* and $\Delta\varphi$ values, the value of the transverse velocity spread $\delta v_\perp$ obtained in the calculations was found to approximately coincide with the corresponding value of velocity spread determined in experiments with hexaboride lanthanum cathode in the SPbPU gyrotron [17].

An important aspect of the simulation discussed in this study is implementation of a sectioned cathode. Two azimuthal sectors without electron emission were symmetrically located on the emissive strip. This cathode sectioning allowed for a significant reduction of parasitic effects near toroidal solenoid bundles used to create an azimuthal magnetic field in the collector region, which affect efficiency of residual electron energy recovery and electron reflection from the collector (see Section III). In the previous simulations [16], the length of each cathode gap sector in azimuthal direction was $\Delta\theta = 70°$. In this study, $\Delta\theta$ was decreased to 45° as a result of optimization of 4-stage collector geometry and operating regimes compared to the original version described in Ref. [16]. Calculations in the electron optical system were performed using Particle Tracking Solver, with number of emission points at the cathode set to 2700. To minimize parasitic effect of mesh step on parameters of high-energy beam, particularly on electron energy spread, a tetrahedral meshing of calculation domain was used.

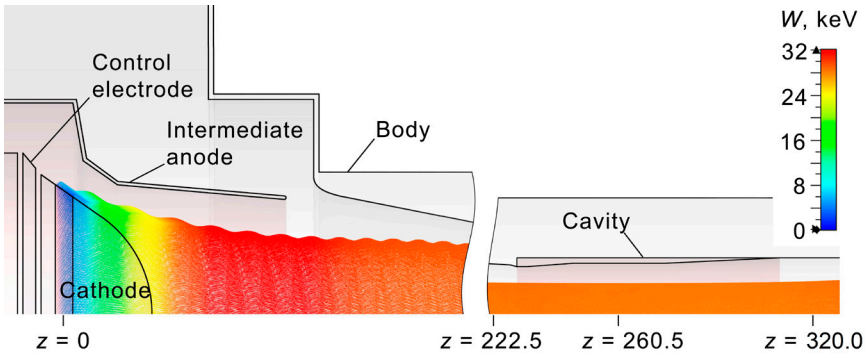

Fig. 1. Schematic drawing of the gyrotron model in the $r - z$ plane with beam trajectories

Table 1

The main geometric parameters of the gyrotron and the characteristics of its operating regime

Parameter, notation, unit	Value
Accelerating voltage U_0, kV	30
Beam current I_b, A	10
Magnetic field induction in the cavity center B_0, T	2.75
Magnetic field induction at the cathode B_c, T	0.152
Operating mode	$TE_{12,3}$
Operating frequency f_0, GHz	74.2
Cavity radius R_0, mm	14.45
Average radius of the cathode emissive strip R_c, mm	35.00

In the experimental gyrotron, magnetic compression coefficient B_0/B_c varies as a result of change in a number of turns of cathode coil [13]. The highest microwave output power in simulations was achieved at $B_0/B_c = 17.01$, which corresponds to 26 turns of cathode coil. In this case, an average beam radius in the cavity was approximately 8.5 mm. In the optimized regime with $T^* = 67\,000$ K, $\Delta\varphi = \pm 90°$, $\Delta\theta = 45°$, $B_0/B_c = 17.01$, $U_a = 7.85$ kV and $U_{cont} = -14.5$ kV, an average pitch factor value α of 1.56 and a transverse velocity spread $\delta v_\perp$ of 5.32 % were provided. The values of velocity and energy spreads were defined as relative standard deviations from the average value of corresponding quantities. The accelerating voltage U_0, the magnetic field induction in the cavity center B_0 and the beam current I_b had values listed in Table I. In this regime, one of 2700 electron trajectories was reflected from the magnetic mirror, resulting in a reflection coefficient K_{ref} of approximately $4 \cdot 10^{-4}$.

Note that, if we assume a Gaussian distribution of the electron velocities, for $\alpha = 1.56$ and $\delta v_\perp = 5.32\%$, the reflection coefficient from the magnetic mirror is $K_{ref} = 2.1 \cdot 10^{-4}$ [13]. It should be noted that reflection of electrons from the magnetic mirror limits an increase in the average pitch factor in the presence of the electron velocity spread. If the coefficient K_{ref} exceeds threshold value, the parasitic low-frequency oscillations (LFOs) can occur in the electron space charge trapped between the cathode and cavity. These oscillations lead to a degradation of the HEB quality [14, 20 – 22]. Based on the experimental data of the SPbPU gyrotron, the threshold value of the reflection coefficient from the magnetic mirror was determined as approximately equal to $1.7 \cdot 10^{-3}$. In the gyrotron operating regime described above, the reflection coefficient was lower than this threshold value. Values of an average pitch factor α and the transverse velocity spread $\delta v_\perp$ in the case of homogeneous emission from the cathode in the described operating regime were 1.57 and 5.21 %, respectively. Therefore, it can be concluded that there was no significant change in these HEB parameters in the case of transition from a homogeneous to a sectioned distribution of emission from the cathode.

Fig. 2 presents the data characterizing particle distribution in the central plane of cavity at $z = 260.5$ mm. Azimuthal positions of the HEB sectors with no electrons correspond to angle ranges of $115° < \theta < 157°$ and $295° < \theta < 337°$, where $\theta = 0°$ coincides with positive x-axis direction (see Fig. 2,*a*). As a result of the crossed electric and magnetic fields, these sectors experienced an azimuthal shift of approximately 18° in clockwise direction viewed along propagation of the HEB moving from the cathode to the cavity. An average potential depression due to the space charge ΔU is about 1.8 kV, with its minimum value located in the HEB areas adjacent to sectors without electrons (see Fig. 2,*a*). The energy spread δW, which is about 0.5 %, is mainly due to nonuniformity of the ΔU distribution in azimuthal direction. In comparison, the similar regime of the gyrotron operation with the homogeneous HEB is characterized by $\delta W = 0.1$ %. Under the action of the crossed azimuthal electric and longitudinal magnetic fields (diocotron effect), particles in areas close to the sectors without electrons move in the radial direction.

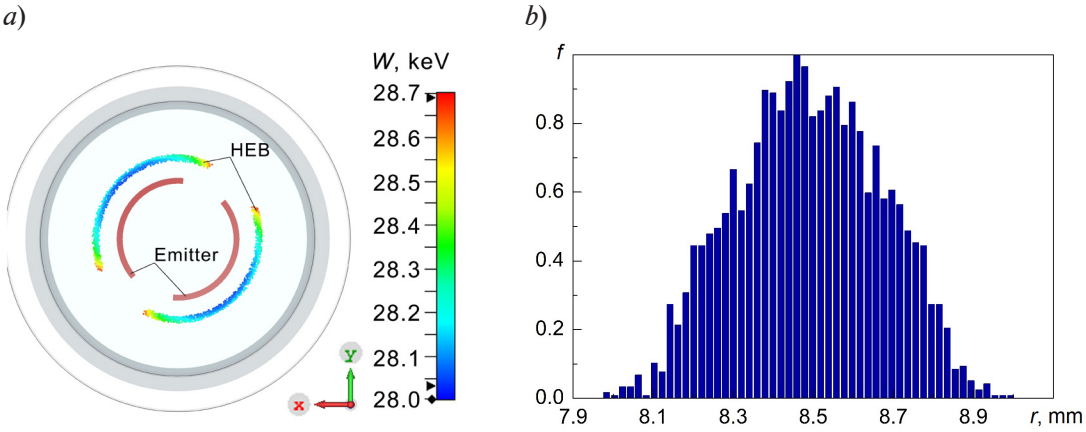

Fig. 2. Simulation results for particle distributions in the central plane of the cavity at $z = 260.5$ mm: positions of HEB particles with energy W in the $x - y$ plane (*a*) and the histogram of the particle radial positions (*b*).
Azimuthal positions of nonemitting sectors on the cathode are shown in Fig. 2,*a*

This movement causes an increase in the HEB wall thickness ΔR_b. As shown in Fig. 2,*b*, ΔR_b is approximately equal to 1 mm if it is determined by the full width of the distribution $f(r)$. In this regime, the radial spread of the leading Larmor centers is $\Delta R_g \approx 0.7$ mm, and the average Larmor radius is $r_1 \approx 0.17$ mm. In Ref. [23], it was shown that ΔR_g in a cavity should not exceed $\lambda/6$, where λ represents a wavelength of microwave radiation. The efficiency of an operating mode generation decreases and there is a possibility of exciting parasitic modes if a value of ΔR_g exceeds this limit.

During the electron-optical system analysis, a special Particle Export Interface Monitor was employed to collect data including the velocities and coordinates of particles in the plane $z = 222.5$ mm (see Fig. 1). Subsequently, this monitor's output was used as an input interface for simulation in the gyrotron cavity.

II. Microwave cavity

The interaction of an electron beam with the electromagnetic field in the cavity of the SPbPU gyrotron was simulated using PIC Solver. Calculation domain was defined by the planes $z = 222.5$ mm and $z = 320$ mm (see Fig. 1). The cavity with a regular part length of 28 mm and a radius of 14.45 mm was designed for the operating $TE_{12,3}$ mode. Simulation results indicated that the maximum output microwave power in the operating mode was achieved at $B_0 = 2.747$ T. The results discussed below were obtained at this magnetic field induction value.

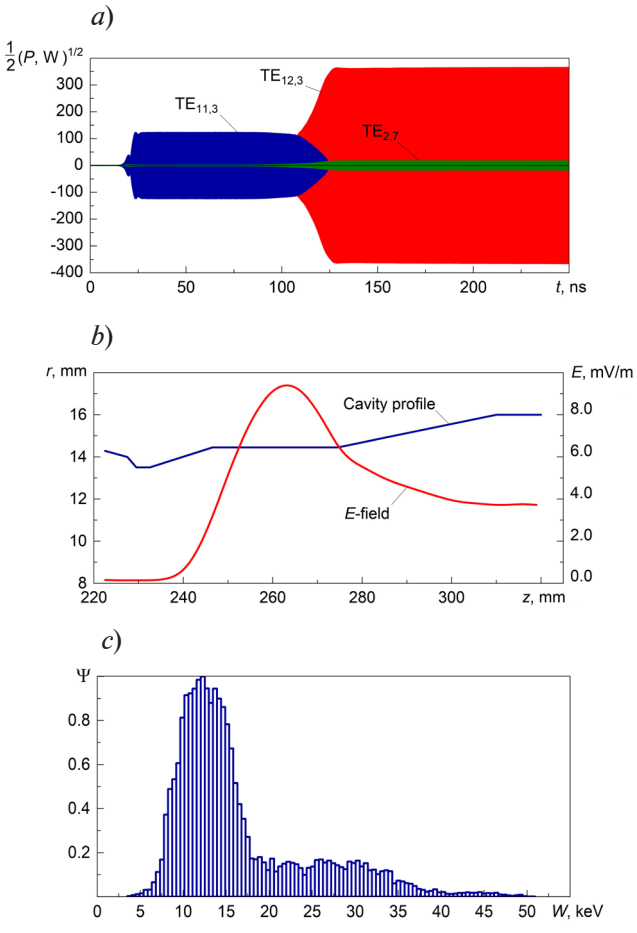

Fig. 3. Simulation results for interaction of an electron beam with the electromagnetic field in the cavity: (*a*) the time dependencies of signals of different modes in the output port ($z = 320$ mm); (*b*) the distributions of the wall radius r and the maximum E-value at 74.5 GHz along the z-axis; (*c*) electron energy spectrum of the spent beam (Ψ – normalized probability density, W – energy)

Fig. 3,*a* illustrates the time variation of the mode signals with the largest amplitude. It can be seen that there are two stable generation regions, namely, the former is with a time interval from 20 to 100 ns and the latter is with a time interval from approximately 130 ns to the simulation end at 250 ns. At $t = 100$ ns and 250 ns, the average output power values of P_{RF} are 15.5 kW and 134.8 kW, respectively. These two regions are distinguished by their mode composition in the cavity. In the first excitation region, the $TE_{11,3}$ mode with an azimuthal index one less than for the operating mode excited at a frequency of 71.5 GHz. Over time, this mode is suppressed simultaneously with excitation of the operating mode $TE_{12,3}$ at a frequency of 74.5 GHz. In the same time interval, the excitation of the parasitic mode $TE_{2,7}$ is also observed. Resonant frequencies of operating $TE_{12,3}$ and parasitic $TE_{2,7}$ modes were calculated using the Eigenmode Solver in CST Studio Suite and were equal to 74.83 and 74.94 GHz, respectively. All modes exhibit two polarization components, and each with approximately the same amplitudes, resulting in the circular wave polarization within the cavity.

At time $t = 250$ ns, the high-frequency power $P_{TE_{12,3}} = 133.9$ kW in the operating mode, and $P_{TE_{2,7}} = 0.3$ kW in the parasitic mode (see Fig. 3,*a*). One can also observe that the power ratio between operating and parasitic modes can be affected by the quality

of mesh in the calculation model. We compared the power values of operating and parasitic modes obtained for sectioned and homogeneous HEBs under the same gyrotron operating regime and mesh settings. For the homogeneous HEB, the power values P_{RF} = 138.7 kW, $P_{TE_{12,3}}$ = 137.6 kW, and $P_{TE_{2,7}}$ = 0.2 kW. Thus, the HEB sectioning has a detrimental effect on the beam quality resulting in a decrease of total output power and an increase in the parasitic mode power. Nonetheless, this change in power is negligible, and the efficiency of the converting electron energy into the high-frequency field energy remains considerably high for the case of sectioned HEB. Specifically, at P_{RF} = 134.8 kW, U_0 = 30 kV, I_b = 10 A, the electronic efficiency η_{el} is determined to be 44.9 %. The data on trajectory analysis and PIC simulation in the cavity for uniform and sectioned electron beams are combined in Table 2.

Table 2

Comparison of the simulation results for homogeneous and sectioned helical electron beams

Parameter, notation, unit	Helical electron beam (HEB)	
	Homogeneous	Sectioned
HEB parameters in the central plane of the cavity (trajectory analysis)		
Beam current I_b, A	10	10
Average pitch factor α	1.57	1.56
Transverse velocity spread $\delta v_\perp$, %	5.21	5.32
Energy spread δW, %	0.1	0.5
Beam wall thickness ΔR_b, mm	1.00	0.75
Coefficient of reflection from magnetic mirror K_{ref}	–	$4 \cdot 10^{-4}$
Output radiation parameters (PIC simulation in the cavity)		
Average output power P_{RF}, kW	138.7	134.8
Power of the operating mode $P_{TE_{12,3}}$, kW	137.6	133.9
Electronic efficiency η_{el}, %	46.2	44.9

Fig. 3,*b* presents a graph depicting the variation of E-field maximum amplitude at a frequency of 74.5 GHz with respect to longitudinal coordinate. The profile of the cavity $r(z)$ is also shown in Fig. 3,*b*. In the cone transition region after regular part of the cavity, where the high-frequency field converts into a traveling electromagnetic wave, an interaction occurs between the electrons and this wave, which is referred to as aftercavity interaction. It is known that this interaction causes an alteration in spent HEB energy spectrum, leading to a decrease in minimum electron energy [24]. The electron energy distribution of spent HEB, in turn, influences the maximum total efficiency that can be achieved through implementation of collector systems with residual energy recovery.

Particle 2D Monitor located in the z = 320 mm plane recorded data on the coordinates, velocities, and macro-charge of particles in the spent HEB required for trajectory analysis in the collector region. The monitor collected particle parameters during time interval $\Delta t = 3 \cdot 10^{-3}$ ns, resulting in an output file containing information on approximately $2 \cdot 10^4$ particles for every moment in time t. The energy spectrum obtained after processing of monitor data for t = 250 ns is presented in Fig. 3,*c*. The minimum electron energy is approximately equal to 15 % of eU_0. There is a noticeable number of accelerated particles with an energy exceeding eU_0 value. The electronic efficiency η_{el} can be estimated by known energy spectrum $f(W)$ using the formula

$$\eta_{el} = 1 - \frac{\int_0^\infty f(W) W dW}{eU_0}, \quad (1)$$

where $\int_0^\infty f(W)dW = 1$.

The efficiency obtained for the spectrum is η_{el} = 44.9 %, which matches the efficiency value obtained from the output microwave power.

III. Collector

Collector design. Recovery of the spent beam energy in the SPbPU gyrotron collector is based on spatial separation of HEB electron fractions with different energies in the crossed longitudinal electric E_z and azimuthal magnetic B_θ fields [12]. Previously, collectors with multistage recovery based on this method were developed for various gyrotrons [16, 25 – 27]. These collectors utilize a toroidal-type solenoid with outer and inner winding for generation of azimuthal magnetic field. Unlike multistage collectors with non-adiabatic fields (see, for example, Refs. [28 – 31]) or collectors with azimuthal electric field (see, for example, Refs. [10, 11]), the developed collectors have extended region with crossed E_z and B_θ fields, which allows to reduce negative influence of velocity and positional spreads of electrons and uncontrolled misalignment of electrodes and magnetic coils on collector efficiency.

The upgraded collector described in this paper differs from its original version presented in Ref. [16] by modified geometry of magnetic coils and collector sections. The data from simulation of similar collector for prototype gyrotron of the DEMO project [27] was used for modernization of the collector for the SPbPU gyrotron. The main elements of the collector for the SPbPU gyrotron are presented in Fig. 4. The cylindrical part of the collector body contains sections S1 – S4 under negative potentials used to create an electric field. Correcting coils C1 – C5, in combination with the gyrotron magnetic system including the main coil, cathode and collector ones, provide required distribution of longitudinal magnetic field. A toroidal solenoid is used to create an azimuthal magnetic field. The end conductors of this solenoid, from the side closest to the cavity, are assembled into two radial bundles located in the tubes providing connection of inner and outer winding. The inner radius of cylindrical part of the collector body is 104.5 mm. The longitudinal coordinate z corresponding to the end of transition from a conical part to cylindrical one of the collector is 667 mm. The coordinate z corresponding to the middle of connecting tubes with bundles is 619 mm. The described collector system has been already equipped in the SPbPU gyrotron. The sectioned emitter for the gyrotron was created by mechanically removing two azimuthal sectors, 45° each, from lanthanum hexaboride emissive strip on the cathode.

Optimization of magnetic field distribution in the collector region. During the process of searching for the optimal distribution of the magnetic field, adjustments were made to geometry and currents of the toroidal solenoid and the correcting coils C1 – C5. Originally, trajectories of "single" electrons starting in the plane z = 320 mm were analyzed. The initial energy and radial coordinate of these electrons were equal to 20 keV and 9 mm respectively. The initial azimuthal coordinate θ was varied. Fig. 5 shows projections of electron trajectories on the r–z

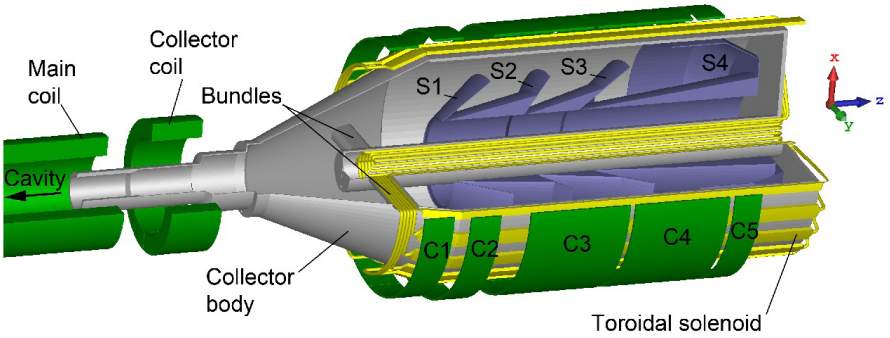

Fig. 4. Schematic drawing of the gyrotron collector region:
S1 – S4 are sections under negative potentials, C1 – C5 are correcting coils

plane for different values of θ from 0° to 180° (Fig. 5,*a*) and longitudinal distributions of different components of magnetic field (Fig. 5,*b*) obtained after optimization. The relative position of the electron emission points with regard to toroidal solenoid bundles can also be seen in Fig. 5,*a*. The bundles are located in the planes θ = 90° and 270°. Due to system symmetry, the electron trajectories in the range of θ from 180° to 360° will coincide with those shown in Fig. 5,*a*. Potentials of the collector sections were set to zero during these calculations.

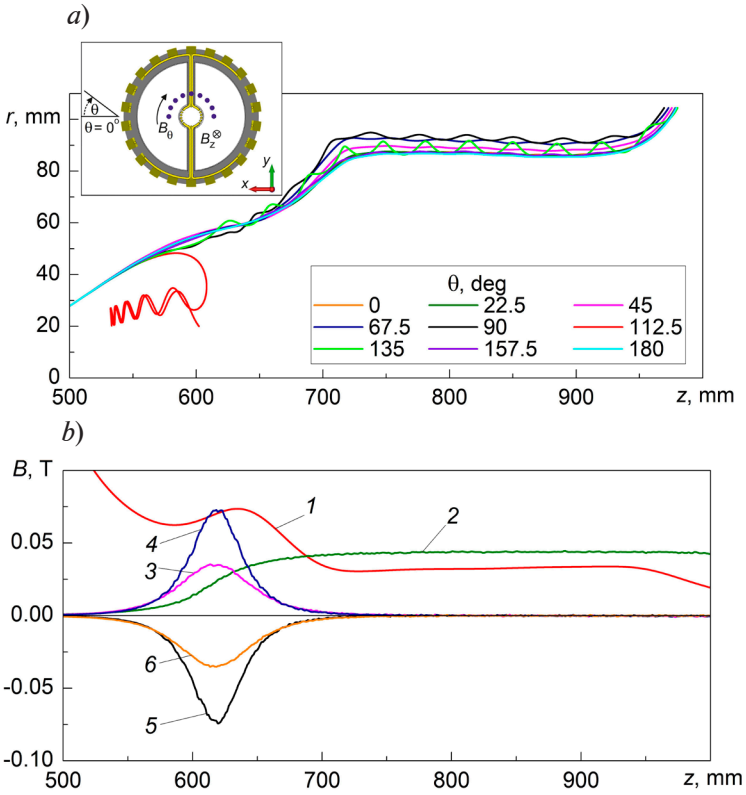

Fig. 5. Simulation results for search for the optimal distribution of the magnetic field *B*: (*a*) projections of electron trajectories with different azimuthal coordinates θ of the starting point; (*b*) the distributions of the *B*-field components (*B*-comps) along the *z*-axis.

Fig 5,*a*: there are azimuthal positions of the starting point of electrons and the bundles of toroidal solenoid in the $x - y$ plane.

Fig 5,*b*: there is data on the axial *B*-comp created by the main gyrotron magnetic system and correcting coils (*1*) as well as azimuthal (*2*) and axial (*3*–*6*) *B*-comps of the toroidal solenoid; the data was obtained at different coordinate values of *r*, mm and θ, degs:

80, 0.0 (*1*, *2*); 60, 45.0 (*3*); 60, 67.5 (*4*); 60, 112.5 (*5*); 60, 135.0 (*6*)

The efficient operation of the multistage collector requires minimizing the spread of radial positions of electron trajectories with different azimuthal coordinates at the collector entry in the absence of voltages on sections. Calculations for the DEMO gyrotron [27] showed that a decrease in the radial spread can be achieved by selecting a positive direction of the azimuthal magnetic field (see Fig. 5,*a*). The decrease can also be achieved by choosing a required magnetic induction value of the main gyrotron magnetic system and correcting coils in the area of toroidal solenoid bundles at $z \approx 620$ mm. The optimized distribution of magnetic field provides the small radial position spread in the recovery region ($z > 700$ mm), where the induction of longitudinal magnetic field B_z is approximately equal to 0.032 T and the azimuthal field B_θ is approximately 0.044 T at $r = 80$ mm.

However, after optimization, the certain number of electrons which propagate near the bundles of the toroidal solenoid are still present, and their trajectories are noticeably perturbed under the action of bundles' parasitic field. These electrons cannot reach the sections with potentials corresponding to their energies and settle on other electrodes of the collector. Alternatively,

they may be reflected from the collector towards the cavity, reducing electronic efficiency. In either scenario, the total gyrotron efficiency is diminished. For example, an electron with the initial coordinate $\theta = 112.5°$ settles on the connecting tube in which the bundle is located (see Fig. 5,*a*). It can be seen that the total longitudinal magnetic field determined by the sum of B_z values at azimuth $\theta = 112.5°$ (curves *1* and *5*) is close to zero in the bundle region (see Fig. 5,*b*). To address this issue, the HEB was sectioned as described in Sections I and II to eliminate negative influence of such electrons on operation of the multistage collector. An additional displacement of the HEB in azimuthal direction during its movement between the planes $z = 260.5$ and 320 mm was insignificant and did not exceed 1°.

For further calculations, the toroidal solenoid was rotated 19° clockwise to achieve a minimum reflection of particles from the collector due to parasitic action of the magnetic field created by bundles' conductors.

Trajectory analysis in the collector with four-stage energy recovery. In the case of ideal separation, each fraction of spent HEB with energy W is deposited on the section under the most negative potential, the modulus of which does not exceed eW (e is the electron charge), and the collector body is under zero potential. The dependency of maximum total efficiency of the SPbPU gyrotron η_{max} achieved with ideal separation on the number of recovery stages N was calculated before the collector modeling. The spectrum of spent HEB shown in Fig. 3,*c* was used. For this calculation, the spectrum was divided into 1000 intervals with different energies. 1 % of the HEB current with electrons having the lowest energy was assumed to be reflected from the collector. The maximum total efficiency was achieved at optimal potentials of the sections U_i ($i = 1, 2, ..., N$) determined through iterations over the values of these potentials with a step of 0.2 kV. As in previous studies presented in [16, 25 – 27], the choice of four stages is dictated by a balance between the achieving maximum total efficiency of the gyrotron and practical difficulties associated with implementing a recovery system with a large number of stages. It should be noted that an increase in the number of collector sections does not substantially complicate the design of the described collector, unlike other designs with nonadiabatic fields [28 – 31].

Four cone-shaped sections are located in the cylindrical part of collector body (see Fig. 4). Changes in geometry of these sections compared with the original design described in Ref. [16] are due to modifications made to the collector magnetic system. Specifically, the direction of azimuthal magnetic field was changed to positive (see Fig. 5,*a*), so the sections were located in the region of smaller radii along the direction of electron drift in the crossed E_z and B_θ fields.

It should be noted that in the regime in the absence of the azimuthal magnetic field and zero voltage on the collector sections, the beam wall thickness in recovery region ($z > 700$ mm) is approximately 10 mm. With optimized distributions of azimuthal and axial magnetic fields and the length of the cathode's sectors without emission of 45° in the absence of voltages on the sections, approximately 94 % of the particles reached the final Section S4, 5 % deposited on the collector body, and less than 1 % deposited on Sections S1 – S3.

During a trajectory analysis in the collector, a Particle Import Interface was placed at the input plane $z = 320$ mm. It contained an array of particles that was determined during the simulation in the gyrotron cavity (as described in Section II). The initial potentials of collector sections $U_{S1} - U_{S4}$ were set equal to the optimal values obtained with ideal separation. Subsequently, through a series of electron trajectory calculations of spent HEB in the collector, these potential values were adjusted to achieve the maximum total efficiency of the gyrotron with an electron reflection coefficient from the collector less than 1 %. At $U_{S1} = -7.1$ kV, $U_{S2} = -10.7$ kV, $U_{S3} = -14.3$ kV, $U_{S4} = -25.2$ kV and $U_{coll} = 0$, the power dissipated over the collector sections and the body was $P_{S1} = 6.2$ kW, $P_{S2} = 6.2$ kW, $P_{S3} = 11.7$ kW, $P_{S4} = 10.2$ kW, and $P_{coll} = 1.2$ kW respectively, with the collector reflection coefficient of 0.99 %. Consequently, the total power P_{diss} dissipated on collector was 35.5 kW. At power $P_{RF} = 134.8$ kW, the total efficiency was

$$\eta_t = \frac{P_{RF}}{P_{RF} + P_{diss}} = 79.2\ \%, \qquad (2)$$

and the collector efficiency was

$$\eta_t = 1 - \frac{P_{diss}}{U_0 I_b - P_{\mathrm{RF}}} = 78.5\ \%. \qquad (3)$$

Thus, through optimization of the magnetic field distribution and the collector sections' geometry, the total efficiency over 79 % was achieved. This value is about 2 % less than the maximum efficiency in a four-stage recovery system with ideal separation of electrons with different energies. For comparison, the total efficiency was 71.8 % in the initial version of the collector for the SPbPU gyrotron [16].

Fig. 6 shows positions of particles in the $x - z$ plane, obtained as a result of intersection of the HEB trajectories with this plane. The picture demonstrates the drift of electrons in the radial direction by the action of crossed E_z and B_θ fields while propagating in the retarding electric field in the recovery region. The direction of field B_θ causes the drift towards smaller radii. Some of the electrons are deposited on the back walls of sections after changing their longitudinal movement direction. As the initial energy of electrons increases, they propagate a greater distance along the z-axis and deposit on sections with a more negative potential.

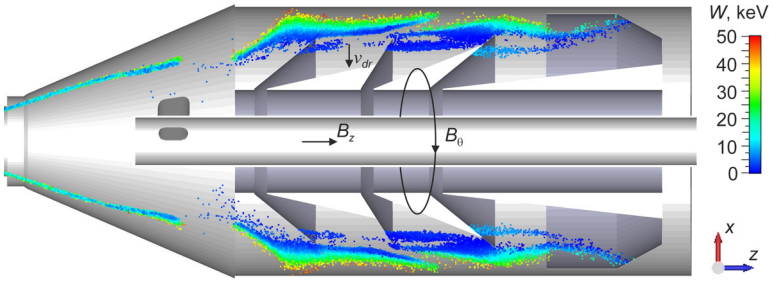

Fig. 6. Positions of particles in the plane x–z (the color corresponds to the particle energy W). The directions of the longitudinal B_z and the azimuthal B_θ magnetic fields and the electron drift velocity v_{dr} are shown

Conclusion

The present study consisted of complex simulation to investigate the possibility of achieving record values of the total efficiency for a moderate-power gyrotron operating in 4 mm wavelength range. High efficiency was achieved by enhancement of the HEB quality in the electron optical system and by recovering the residual electron energy using a multistage collector system. Parameters of the spent HEB were determined through a trajectory analysis in the electron optical system taking into account the spread of initial electron velocities at the cathode and simulation of interaction of formed HEB with a high-frequency field in the gyrotron cavity. Spatial separation of electron fractions with different energies in the collector was achieved using a method based on electron drift in the crossed longitudinal electric and azimuthal magnetic fields. A toroidal solenoid was used as a source of the azimuthal magnetic field. The end conductors of toroidal solenoid were assembled in bundles to increase the number of electrons passing to the recovery area. The negative influence of the magnetic field created by these bundles on the collector efficiency and the electron reflection coefficient was reduced through the sectioning of the electron beam.

It is important to underline the main differences between this study and the one described in Ref. [16] where the former version of the four-stage recovery collector for the SPbPU gyrotron was analyzed. In this study, a trajectory analysis in the electron optical system of the gyrotron has been performed considering the initial velocity spread of electrons on a cathode. As a consequence, characteristics of the beam entering the resonator, output radiation parameters, and, importantly for collector modeling, the spent electron beam parameters have undergone changes. The main distinction from Ref. [16] lies in the modification of the collector system's design. Alteration of the azimuthal magnetic field direction and optimization of the longitudinal magnetic field distribution using correcting coils enabled reducing the radial trajectory spread in the recovery region. Single-electron trajectory calculations in the collector region were employed for this purpose. The collector sections feature a new geometry, and their potentials were selected based on calculations of the maximum total efficiency with ideal separation of electrons of different energies. Compared to the results of Ref. [16], performed modernization of the collector

for the SPbPU gyrotron allowed for an increase in calculated total efficiency from 71.8 to 79.2 % with a reflection coefficient from the collector of less than 1 % and for a reduction of the length of cathode gap sectors where emission is absent, from 70 to 45°. With incorporation of the new simulation data described in this work, an upgraded version of the collector for the SPbPU gyrotron has been manufactured.

Continuation of this work may involve further improvement of the azimuthal magnetic field source, which will simplify the design of the collector.

REFERENCES

1. **Thumm M. K. A., Denisov G. G., Sakamoto K., Tran M. Q.,** High-power gyrotrons for electron cyclotron heating and current drive, Nucl. Fusion. 59 (7) (2019) 073001.

2. **Thumm M.,** State-of-the-art of high-power gyro-devices and free electron masers, J. Infrared Millim. Terahertz Waves. 41 (1) (2020) 1–140.

3. **Litvak A. G., Denisov G. G., Myasnikov V. E., et al.,** Development in Russia of megawatt power gyrotrons for fusion, J. Infrared Millim. Terahertz Waves. 32 (3) (2011) 337–342.

4. **Darbos C., Albajar F., Bonicelli T., et al.,** Status of the ITER electron cyclotron heating and current drive system, J. Infrared Millim. Terahertz Waves. 37 (1) (2016) 4–20.

5. **Jelonnek J., Aiello G., Alberti S., et al.,** Design considerations for future DEMO gyrotrons: A review on related gyrotron activities within EUROfusion, Fusion Eng. Des. 123 (November) (2017) 241–246.

6. **Sakamoto K., Tsuneoka M., Kasugai A., et al.,** Major improvement of gyrotron efficiency with beam energy recovery, Phys. Rev. Lett. 73 (26) (1994) 3532–3535.

7. **Glyavin M. Y., Kuftin A. N., Venediktov N. P., Zapevalov V. E.,** Experimental investigation of a 110 GHz/1 MW gyrotron with the one-step depressed collector, Int. J. Infrared Millim. Waves. 18 (11) (1997) 2129–2136.

8. **Manuilov V. N., Morozkin M. V., Luksha O. I., Glyavin M. Y.,** Gyrotron collector systems: Types and capabilities, Infrared Phys. Technol. 91 (June) (2018) 46–54.

9. **Pagonakis I. Gr., Hogge J.-P., Alberti S., et al.,** A new concept for the collection of an electron beam configured by an externally applied axial magnetic field, IEEE Trans. Plasma Sci. 36 (2) (2008) 469–480.

10. **Wu C., Pagonakis I. G., Avramidis K. A., et al.,** Gyrotron multistage depressed collector based on E×B drift concept using azimuthal electric field. I. Basic design, Phys. Plasmas. 25 (3) (2018) 033108.

11. **Ell B., Wu C., Gantenbein G., et al.,** Toward the first continuous wave compatible multistage depressed collector design for high power gyrotrons, IEEE Trans. Electron Devices. 70 (3) (2023) 1299–1305.

12. **Louksha O. I., Trofimov P. A.,** A method of electron separation for multistep recuperation systems in gyrotrons, Tech. Phys. Lett. 41 (9) (2015) 884–886.

13. **Louksha O. I., Piosczyk B., Sominski G. G., et al.,** On potentials of gyrotron efficiency enhancement: measurements and simulations on a 4-mm gyrotron, IEEE Trans. Plasma Sci. 34 (3) (2006) 502–511.

14. **Louksha O. I., Samsonov D. B., Sominskii G. G., Semin S. V.,** Dynamic processes in helical electron beams in gyrotrons, Tech. Phys. 58 (5) (2013) 751–759.

15. **Louksha O. I., Sominski G. G., Arkhipov A. V., et al.,** Gyrotron research at SPbPU: Diagnostics and quality improvement of electron beam, IEEE Trans. Plasma Sci. 44 (8) (2016) 1310–1319.

16. **Louksha O. I., Trofimov P. A.,** Highly efficient gyrotron with multi-stage recuperation of residual electron energy, Tech. Phys. 64 (12) (2019) 1889–1897.

17. **Louksha O. I., Trofimov P. A., Malkin A. G.,** Trajectory analysis in a gyrotron electron-optical system with allowance for the cathode surface roughness, Radiophys. Quant. El. 65 (3) (2022) 209–218.

18. **Louksha O. I., Trofimov P. A.,** Simulation of non-uniform electron beams in the gyrotron electron-optical system, Tech. Phys. 63 (4) (2018) 598–604.

19. **Louksha O. I., Samsonov D. B., Sominskii G. G., Tsapov A. A.,** Improvement of the helical electron beam quality and the gyrotron efficiency by controlling the electric field distribution near a magnetron injection gun, Tech. Phys. 57 (6) (2012) 835–839.

20. **Tsimring Sh. E.,** Gyrotron electron beams: velocity and energy spread and beam instabilities, Int. J. Infrared Millim. Waves. 22 (10) (2001) 1433–1468.

21. **Manuilov V. N.,** Numerical simulation of low-frequency oscillations of the space charge and potential in the electron-optical system of a gyrotron, Radiophys. Quant. El. 49 (10) (2006) 786–792.

22. **Louksha O. I.,** Simulation of low-frequency collective processes in gyrotron electron beams, Radiophys. Quant. El. 52 (5–6) (2009) 386–397.

23. **Pu R., Nusinovich G. S., Sinitsyn O. V., Antonsen T. M. Jr.,** Effect of the thickness of electron beams on the gyrotron efficiency, Phys. Plasmas. 17 (8) (2010) 083105.

24. **Zapevalov V. E., Moiseev M. A.,** Influence of aftercavity interaction on gyrotron efficiency, Radiophys. Quant. El. 47 (7) (2004) 520–527.

25. **Louksha O. I., Trofimov P. A.,** A multistage depressed collector system for gyrotrons, Proc. 18th Int. Vacuum Electronics Conf. (IVEC), April 24–26, London, UK (2017) 1–2.

26. **Louksha O. I., Trofimov P. A., Manuilov V. N., Glyavin M. Yu.,** Trajectory analysis in a collector with multistage energy recovery for a DEMO prototype gyrotron. Part I. Idealized magnetic field distribution, Tech. Phys. 66 (1) (2021) 118–123.

27. **Louksha O. I., Trofimov P. A., Manuilov V. N., Glyavin M. Yu.,** Trajectory analysis in a collector with multistage energy recovery for a DEMO prototype gyrotron. Part II. Toroidal magnetic field, Tech. Phys. 66 (8) (2021) 992–998.

28. **Read M. E., Lawson W. G., Dudas A. J., Singh A.,** Depressed collectors for high-power gyrotrons, IEEE Trans. Electron Devices. 37 (6) (1990) 1579–1589.

29. **Singh A., Rajapatirana S., Men Y., et al.,** Design of a multistage depressed collector system for 1-MW CW gyrotrons. I. Trajectory control of primary and secondary electrons in a two-stage depressed collector, IEEE Trans. Plasma Sci. 27 (2) (1999) 490–502.

30. **Ling G., Piosczyk B., Thumm M. K.,** A new approach for a multistage depressed collector for gyrotrons, IEEE Trans. Plasma Sci. 28 (3) (2000) 606–613.

31. **Glyavin M. Y., Morozkin M. V., Petelin M. I.,** Separation of energy fractions of an electron beam by a localized nonuniformity of magnetic field in the collector region of gyrodevices, Radiophys. Quant. El. 49 (10) (2006) 811–815.

СПИСОК ЛИТЕРАТУРЫ

1. **Thumm M. K. A., Denisov G. G., Sakamoto K., Tran M. Q.** High-power gyrotrons for electron cyclotron heating and current drive // Nuclear Fusion. 2019. Vol. 59. No. 7. P. 073001.

2. **Thumm M.** State-of-the-art of high-power gyro-devices and free electron masers // Journal of Infrared, Millimeter, and Terahertz Waves. 2020. Vol. 41. No. 1. Pp. 1–140.

3. **Litvak A. G., Denisov G. G., Myasnikov V. E., Tai E. M., Azizov E. A., Ilin V. I.** Development in Russia of megawatt power gyrotrons for fusion // Journal of Infrared, Millimeter, and Terahertz Waves. 2011. Vol. 32. No. 3. Pp. 337–342.

4. **Darbos C., Albajar F., Bonicelli T., et al.** Status of the ITER electron cyclotron heating and current drive system // Journal of Infrared, Millimeter, and Terahertz Waves. 2016. Vol. 37. No. 1. Pp. 4–20.

5. **Jelonnek J., Aiello G., Alberti S., et al.** Design considerations for future DEMO gyrotrons: A review on related gyrotron activities within EUROfusion // Fusion Engineering and Design. 2017. Vol. 123. November. Pp. 241–246.

6. **Sakamoto K., Tsuneoka M., Kasugai A., Imai T., Kariya T., Hayashi K., Mitsunaka Y.** Major improvement of gyrotron efficiency with beam energy recovery // Physical Review Letters. 1994. Vol. 73. No. 26. Pp. 3532–3535

7. **Glyavin M. Y., Kuftin A. N., Venediktov N. P., Zapevalov V. E.** Experimental investigation of a 110 GHz / 1 MW gyrotron with the one-step depressed collector // International Journal of Infrared and Millimeter Waves. 1997. Vol. 18. No. 11. Pp. 2129–2136.

8. **Manuilov V. N., Morozkin M. V., Luksha O. I., Glyavin M. Y.** Gyrotron collector systems: Types and capabilities// Infrared Physics & Technology. 2018. Vol. 91. June. Pp. 46–54.

9. **Pagonakis I. Gr., Hogge J.-P., Alberti S., Avramides K. A., Vomvoridis J. L.** A new concept for the collection of an electron beam configured by an externally applied axial magnetic field // IEEE Transactions on Plasma Science. 2008. Vol. 36. No. 2. Pp. 469–480.

10. **Wu C., Pagonakis I. G., Avramidis K. A., Gantenbein G., Illy S., Thumm M., Jelonnek J.** Gyrotron multistage depressed collector based on E×B drift concept using azimuthal electric field. I. Basic design // Physics of Plasmas. 2018. Vol. 25. No. 3. P. 033108.

11. **Ell B., Wu C., Gantenbein G., Illy S., Misko M. S., Pagonakis I. Gr., Weggen J., Thumm M., Jelonnek J.** Toward the first continuous wave compatible multistage depressed collector design for high power gyrotrons // IEEE Transactions on Electron Devices. 2023. Vol. 70. No. 3. Pp.1299–1305.

12. **Лукша О. И., Трофимов П. А.** Метод сепарации электронов для систем многоступенчатой рекуперации в гиротронах // Письма в Журнал технической физики. 2015. Т. 41. № 18. С. 38–45.

13. **Louksha O. I., Piosczyk B., Sominski G. G., Thumm M. K., Samsonov D. B.** On potentials of gyrotron efficiency enhancement: measurements and simulations on a 4-mm gyrotron // IEEE Transactions on Plasma Science. 2006. Vol. 34. No. 3. Pp. 502–511.

14. **Лукша О. И., Самсонов Д. Б., Соминский Г. Г., Сёмин С. В.** Динамические процессы в винтовых электронных потоках гиротронов // Журнал технической физики. 2013. Т. 83. № 5. С. 132–140.

15. **Louksha O. I., Sominski G. G., Arkhipov A. V., Dvoretskaya N. G., Kolmakova N. V., Samsonov D. B., Trofimov P. A.** Gyrotron research at SPbPU: Diagnostics and quality improvement of electron beam // IEEE Transactions on Plasma Science. 2016. Vol. 44. No. 8. Pp. 1310–1319.

16. **Лукша О. И., Трофимов П. А.** Высокоэффективный гиротрон с многоступенчатой рекуперацией остаточной энергии электронов // Журнал технической физики. 2019. Т. 89. № 12. С. 1988–1996.

17. **Лукша О. И., Трофимов П. А., Малкин А. Г.** Траекторный анализ в электронно-оптической системе гиротрона с учетом шероховатости поверхности катода // Известия высших учебных заведений. Радиофизика. 2022. Т. 65. № 3. С. 226–237.

18. **Лукша О. И., Трофимов П. А.** Моделирование неоднородных электронных потоков в электронно-оптической системе гиротрона // Журнал технической физики. 2018. Т. 88. № 4. С. 614–620.

19. **Лукша О. И., Самсонов Д. Б., Соминский Г. Г., Цапов А. А.** Повышение качества винтового электронного потока и кпд гиротрона при регулировании распределения электрического поля в области магнетронно-инжекторной пушки // Журнал технической физики. 2012. Т. 82. № 6. С. 101–105.

20. **Tsimring Sh. E.** Gyrotron electron beams: velocity and energy spread and beam instabilities // International Journal of Infrared and Millimeter Waves. 2001. Vol. 22. No. 10. Pp. 1433–1468.

21. **Мануилов В. Н.** Численное моделирование низкочастотных колебаний пространственного заряда и потенциала в электронно-оптической системе гиротрона // Известия высших учебных заведений. Радиофизика. 2006. Т. 49. № 10. С. 872–879.

22. **Лукша О. И.** Моделирование низкочастотных коллективных процессов в электронных потоках гиротронов // Известия высших учебных заведений. Радиофизика. 2009. Т. 52. № 5–6. С. 425–437.

23. **Pu R., Nusinovich G. S., Sinitsyn O. V., Antonsen T. M. Jr.** Effect of the thickness of electron beams on the gyrotron efficiency // Physics of Plasmas. 2010. Vol. 17. No. 8. P. 083105.

24. **Запевалов В. Е., Моисеев М. А.** Влияние послерезонаторного взаимодействия на кпд гиротрона // Известия высших учебных заведений. Радиофизика. 2004. Т. 47. № 7. С. 584–592.

25. **Louksha O. I., Trofimov P. A.** A multistage depressed collector system for gyrotrons, Proceedings of the 18th International Vacuum Electronics Conference (IVEC), April 24–26, London, UK (2017) 1–2.

26. **Лукша О. И., Трофимов П. А., Мануилов В. Н., Глявин М. Ю.** Траекторный анализ в коллекторе с многоступенчатой рекуперацией энергии для прототипа гиротрона DEMO. Часть I. Идеализированное распределение магнитного поля // Журнал технической физики. 2021. Т. 91. № 1. С. 125–130.

27. **Лукша О. И., Трофимов П. А., Мануилов В. Н., Глявин М. Ю.** Траекторный анализ в коллекторе с многоступенчатой рекуперацией энергии для прототипа гиротрона DEMO. Часть II. Тороидальное магнитное поле // Журнал технической физики. 2021. Т. 91. № 7. С. 1182–1188.

28. **Read M. E., Lawson W. G., Dudas A. J., Singh A.** Depressed collectors for high-power gyrotrons // IEEE Transactions on Electron Devices. 1990. Vol. 37. No. 6. Pp. 1579–1589.

29. **Singh A., Rajapatirana S., Men Y., Granatstein V. L., Ives R. L., Antolak A. J.** Design of a multistage depressed collector system for 1-MW CW gyrotrons. I. Trajectory control of primary and secondary electrons in a two-stage depressed collector // IEEE Transactions on Plasma Science. 1999. Vol. 27. No. 2. Pp. 490–502.

30. **Ling G., Piosczyk B., Thumm M. K.** A new approach for a multistage depressed collector for gyrotrons // IEEE Transactions on Plasma Science. 2000. Vol. 28. No. 3. Pp. 606–613.

31. **Глявин М. Ю., Морозов М. В., Петелин М. И.** Разделение энергетических фракций электронного пучка локализованной неоднородностью магнитного поля в коллекторной области гироприборов // Известия высших учебных заведений. Радиофизика. 2006. Т. 49. № 10. С. 900–905.

THE AUTHORS

LOUKSHA Oleg I.
Peter the Great St. Petersburg Polytechnic University
29 Politechnicheskaya St., St. Petersburg, 195251, Russia
louksha@rphf.spbstu.ru
ORCID: 0000-0002-6402-8112

TROFIMOV Pavel A.
Peter the Great St. Petersburg Polytechnic University
29 Politechnicheskaya St., St. Petersburg, 195251, Russia
trofpa@yandex.ru
ORCID: 0000-0002-3585-1169

MALKIN Alexander G.
Peter the Great St. Petersburg Polytechnic University
29 Politechnicheskaya St., St. Petersburg, 195251, Russia
alexmalkin47@gmail.com
ORCID: 0000-0003-4047-3956

СВЕДЕНИЯ ОБ АВТОРАХ

ЛУКША Олег Игоревич – *доктор физико-математических наук, профессор Высшей инженерно-физической школы Санкт-Петербургского политехнического университета Петра Великого, Санкт-Петербург, Россия.*
195251, Россия, г. Санкт-Петербург, Политехническая ул., 29
louksha@rphf.spbstu.ru
ORCID: 0000-0002-6402-8112

ТРОФИМОВ Павел Анатольевич – *кандидат физико-математических наук, инженер Высшей инженерно-физической школы Санкт-Петербургского политехнического университета Петра Великого, Санкт-Петербург, Россия.*
195251, Россия, г. Санкт-Петербург, Политехническая ул., 29
trofpa@yandex.ru
ORCID: 0000-0002-3585-1169

МАЛКИН Александр Геннадьевич – *студент Института электроники и телекоммуникаций Санкт-Петербургского политехнического университета Петра Великого, Санкт-Петербург, Россия.*

195251, Россия, г. Санкт-Петербург, Политехническая ул., 29
alexmalkin47@gmail.com
ORCID: 0000-0003-4047-3956

Received 09.09.2023. Approved after reviewing 18.09.2023. Accepted 18.09.2023.
Статья поступила в редакцию 09.09.2023. Одобрена после рецензирования 18.09.2023. Принята 18.09.2023.